Astron. Astrophys. 363, 1065–1080 (2000)

ASTRONOMY AND ASTROPHYSICS

H_2 in the 2 micron infrared spectra of long period variables

I. Observations

K.H. Hinkle[1], **B. Aringer**[2], **T. Lebzelter**[2], **C.L. Martin**[1,3], **and S.T. Ridgway**[1]

[1] Kitt Peak National Observatory, National Optical Astronomy Observatories*, 950 N. Cherry Avenue, P.O. Box 26732, Tucson, AZ 85726, USA

[2] Institut für Astronomie, Türkenschanzstrasse 17, 1180 Vienna, Austria

[3] Present Address: STScI, 3700 San Martin Drive, Baltimore, Maryland 21218, USA

Received 11 July 2000 / Accepted 20 July 2000

Abstract. Up to seven lines in the S branch of molecular hydrogen have been detected in the 2 μm infrared absorption line spectra of long period variables. The H_2 lines show very strong phase dependent changes in velocity, equivalent width, and line profile, with the strongest lines near minimum light. The strength of the H_2 lines also depends on variable type with Mira variables having deep lines (at minimum light), SRa variables generally having detectable lines, and the SRb and non-variables having weak to non-detectable lines. In addition H_2 line strengths depend on period and on C/O abundance, with long period (i.e. cool), pure S-type Miras having H_2 lines with central depths of up to 80%. The appearance of H_2 lines in the spectra of cool giants is linked with geometrical extension of the atmosphere. The greatly increased strength of the H_2 lines in Mira variables is observational evidence of the role of stellar pulsation in greatly extending these stellar atmospheres. Weak emission is seen in H_2 near maximum light in Miras. We suggest this is resonant scattering in the spherically extended stellar atmosphere. The significant role of H_2 opacity in the blue is noted.

Key words: line: profiles – stars: AGB and post-AGB – stars: atmospheres – stars: variables: general – infrared: stars

1. Introduction

It has long been recognized that in the coolest stellar atmospheres a significant fraction of the hydrogen forms molecular hydrogen (Tsuji 1964). The dissociation energy of the H_2 molecule is 4.48 eV and in layers cooler than ≈ 2500 K molecular hydrogen is the predominant atmospheric constituent. Nevertheless, spectral lines from molecular hydrogen are notoriously difficult to observe. As noted by Herzberg (1938), this is because homonuclear diatomic molecules such as H_2 have no permitted electric dipole spectrum and hence no permitted rotation or vibration-rotation spectrum. There is a permitted quadrupole spectrum but the lines are weak. In the case of H_2 a typical quadrupole oscillator strength is $3{\cdot}10^{-14}$. By comparison, a typical molecular dipole or atomic oscillator strength in the same spectral region as the H_2 quadrupole lines is 10^6 times larger.

Detection of H_2 lines in cool giant spectra, especially in the spectra of AGB stars, is important for a number of reasons: Due to the large predicted abundance of H_2 in the stellar atmosphere detection of spectral lines allows a definitive test of stellar model atmospheres (Lambert et al. 1973). Planetary nebulae are known in which hydrogen is depleted (Kaler 1985). Since luminous AGB stars are the immediate precursors of planetary nebulae, it would be interesting to investigate the hydrogen abundance in AGB atmospheres. Finally, in the case of Mira variables, H_2 has been shown to be critical in computing the energy dissipated as the pulsation induced shock moves through the atmosphere. H_2 dissociation can absorb up to 50% of the thermal kinetic energy in a shock (Fox & Wood 1985). While H_2 will be present in a cool equilibrium atmosphere, Bowen (1988) argues that H_2 will not be present in Mira atmospheres because the recombination time (through three body collisions) is much longer than the Mira pulsation period.

The quadrupole vibration-rotation lines of H_2 lie near the flux maximum in cool stars and the continuous opacity minimum at 2 μm. The much stronger electronic transitions are situated in the 1200-1500 Å ultraviolet. Since in cool stars the flux is small in the ultraviolet, the infrared is a more practical region in which to look for this molecule. In spite of the expected weakness of the H_2 infrared quadrupole transitions, there have been a number of searches for these lines. These were based on predictions from model atmosphere calculations that H_2 would reach a large enough column density in cool giant atmospheres to be observable (Lambert et al. 1973; Goorvitch et al. 1980). Early attempts found only upper limits resulting in a gross mismatch between predicted and observed equivalent widths, with the predictions far in excess of the observations. With improved observations, H_2 lines were detected in carbon stars (Johnson et al. 1983) and improved models have resulted in a reasonable

Send offprint requests to: K.H. Hinkle (hinkle@noao.edu)

* Operated by the Association of Universities for Research in Astronomy, Inc. under cooperative agreement with the National Science Foundation.

agreement between observation and prediction for the atmospheres of carbon stars (Lambert et al. 1986). However, Tsuji (1983) concluded that H_2 was not convincingly present in the oxygen rich cool giants and that this result was not in agreement with model atmospheres.

In two earlier papers we noted the presence of very strong molecular hydrogen lines in the spectra of the S-type Miras (Hall & Ridgway 1977; Hinkle et al. 1982 [HHR]). These strong H_2 lines in stars with C/O ≈ 1 are generally in agreement with carbon star results showing that equivalent widths of the H_2 S(0) line increase with decreasing effective temperature and increase strongly as C/O approaches unity (Lambert et al. 1986). In this paper we explore in detail the behavior of the H_2 lines as a function of phase in Mira variables and as a function of C/O and effective temperature in cold long period variables (LPVs). Our goal is to establish when and why this useful atmospheric diagnostic can be detected in late type giants.

2. Atomic and molecular data

The vibration-rotation H_2 lines are found through the 1–3 μm region of the infrared spectrum. A comprehensive line list has been compiled by Black & van Dishoeck (1987). The current paper is limited to the 1.5–2.5 μm region, which includes low excitation S and Q-branch H_2 lines. All the Q-branch H_2 lines are in a spectral region heavily blanketed by CO Δv=2 lines and, in the coolest stars with C/O $\lesssim 1$, by stellar H_2O lines. As a result, the Q-branch lines were not investigated. The 1-0 S(0) and S(1) lines are well placed in the 2 μm telluric window ("K-band"), 1-0 S(0) is well removed from any telluric lines, while a few weak (depth $\lesssim$ 10%) telluric lines are near S(1). 1-0 S(2) is in the region of a telluric CO_2 band with telluric lines of about 30% central depth (at 1 airmass) and $\approx 1\,\mathrm{cm}^{-1}$ spacing crossing the rest frequency of the line. The 1-0 S(3), S(4), and S(5) lines are hopelessly blended with strong telluric CO_2 and H_2O lines. The higher excitation 1-0 S(6) and S(7) lines lie well into the 1.8 μm telluric window ("H-band") and both are separated by several wavenumbers from strong telluric lines. More highly vibrationally excited H_2 lines are also in the 1.5–2.5 μm region. The 2-1 S(1) and S(2) lines are both well placed in the K-band.

Bragg et al. (1982) provide excellent laboratory frequencies, with precisions exceeding 0.1 mK, for the 1-0 S(0), S(1), and S(2) lines. For the remaining lines, the frequencies must be calculated from the molecular constants. For these lines we have used the list computed by Black & van Dishoeck (1987). The excitation potentials were computed for the 1-0 band from the constants provided by Jennings et al. (1984). For the 2-1 band the constants of Bragg et al. (1982) were used. Oscillator strengths for H_2 were computed from the Einstein A coefficients of Turner et al. (1977). The 1-0 band values are in excellent agreement with the values compiled using independent input by Lambert et al. (1973). For H_2 it is important to recall that homonuclear diatomic molecules have nuclear spin statistical weights three times larger for odd J lines than for even J lines. Thus 1-0 S(1) is a much stronger transition than 1-0 S(0). The molecular data are presented in Table 1.

Table 1. H_2 Laboratory Line Data

Designation	Frequency (cm^{-1})	Oscillator Strength	Excitation Potential (cm^{-1})
1-0 S(0)	4497.8391	$9.35{\cdot}10^{-14}$	0.0
1-0 S(1)	4712.9054	$5.46{\cdot}10^{-14}$	118.5
1-0 S(2)	4917.0069	$4.44{\cdot}10^{-14}$	354.4
1-0 S(6)	5592.701	$2.22{\cdot}10^{-14}$	2414.9
1-0 S(7)	5720.974	$1.73{\cdot}10^{-14}$	3187.5
2-1 S(1)	4448.958	$8.80{\cdot}10^{-14}$	4273.7
2-1 S(2)	4642.069	$7.01{\cdot}10^{-14}$	4497.8

In addition to the H_2 lines, supporting measurements were made of CO, CN, and atomic Ti lines. The CO frequencies and oscillator strengths are those used by Hinkle et al. (1984). The CO Δv=3 measurements were taken mainly from HSH and Hinkle et al. (1997). In the K band the CO 2-0 R branch lines J=79, 81, 83, 86, and 87 were measured because they are unblended and free of circumstellar contamination (HHR). CN 0-2 red system data were provided by Smith & Lambert (1989). From the extensive Smith and Lambert CN line list a sample of 20 strong, unblended lines in the 4400–4800 cm^{-1} region were selected. The strong Ti lines in the K band were taken as a representative sample of metal lines (Hinkle & Barnes 1979b). Ti frequencies were taken from Forsberg (1987).

3. Observations

High resolution ($\lambda/\Delta\lambda \approx 70000$) 2 μm region spectra of a number of LPV's were observed in the 1980's using the FTS at the 4 meter Mayall telescope at Kitt Peak National Observatory. For about 20 Miras and semiregular (SR) variables, time series spectra with a sampling of about 0.1 in phase or better exist. Most of these observations are described in detail in HHR, HSH, Wallerstein et al. (1985), and Hinkle et al. (1997). Table 2 is a list of spectra that were examined for H_2. As will be discussed below, time series of Mira variable spectra show the H_2 lines to be strongest near minimum light. As a result, phases near minimum light have been selected for the Mira variable spectra in Table 2. Most of the spectra cover the 1.5–2.5 μm region. For some of the fainter stars the spectrum was only observed over the 2.0–2.5 μm region.

For the Mira χ Cygni a sample of spectra covering the entire light cycle is used. For the most part these are observations of HHR. New observations at an apodized resolution of 0.07 cm^{-1} and signal-to-noise ratio approaching 100 have also been obtained and are listed in Table 3. These observations, like the majority of the other data, cover the 1.5 to 2.5 μm region.

The signal-to-noise ratios reported in Tables 2 and 3 are for the peak signal. The peak signal in these spectra typically occurs near 2.2 μm with the signal-to-noise ratio in the 1.5-1.8 μm region less by as much as a factor of two, the actual amount depending on the phase-dependent energy distribution. Fortunately, the peak signal-to-noise region corresponds to the region where the most interesting H_2 lines are found.

Table 2. Minimum light 2 μm spectra. Classification in Column 5 is based on major spectral features in 2 μm region. m+=strong H_2O, m=moderate H_2O, m-=weak H_2O, s=weak H_2O and weak CN, c=strong CN (see text). References (Column 11): (1) HSH, (2) Lambert et al. 1986, (3) Hinkle et al. 1989, (4) Hinkle et al. 1997, (5) Lebzelter et al. 1999, (6) Lebzelter et al. 2000, (7) Wallerstein et al. 1985.

Star	Variable Type	Period (days)	Spectral Type	Class-ification	Date	Julian Date (2440000+)	Phase	Resolution (cm−1)	S/N	Reference
R And	M	409	S6/5e	s	1978 Oct 17	3798.8	0.58	0.07	114	1
X And	M	346	S5/7e	s	1989 Jul 13	7721.0	0.55	0.14	90	
R Aql	M	284	M6.5e	m+	1976 Sep 30	3051.7	0.58	0.12	97	1
V450 Aql	SRb	64	M8	m-	1984 Nov 13	6018.4	—	0.07	85	6
R Aqr	M	387	M7e	m+	1983 Dec 23	5691.6	0.57	0.07	117	3
R Aur	M	458	M6.5e	m-	1976 May 16	2915.3	0.60	0.09	62	4
T Cam	M	374	S5/5e	s	1989 Jul 13	7721.1	0.45	0.14	114	
R Cas	M	431	M7e	m+	1976 Jul 25	2985.1	0.56	0.08	111	1
SV Cas	SRa	276	M6	m-	1984 Nov 13	6018.5	—	0.07	103	4
T Cas	M	445	M7.5e	s	1982 Nov 6	5279.7	0.53	0.07	174	1
W Cas	M	405	SC6/9e	c	1989 Jul 13	7721.1	0.69	0.14	103	
WZ Cas	SRb	186	SC7/10e	c	1979 Jul 6	4061.1	—	0.07	103	2
WZ Cas	SRb	186	SC7/10e	c	1984 Oct 14	5987.9	—	0.07	150	
S Cep	M	487	C7,4	c	1984 Dec 30	6065.5	0.66	0.07	104	
T Cep	M	388	M6.5e	m-	1977 Feb 19	3194.3	0.53	0.08	68	1
o Cet	M	332	M5.5e	m	1985 Jan 1	6067.5	0.69	0.08	80	1
χ Cyg	M	407	S7/1e	s	1986 Feb 17	6479.1	0.54	0.07	112	1
LX Cyg	M	465	SC7/9e	c	1984 Oct 14	5987.7	0.59	0.14	101	
R Cyg	M	426	S6/6e	s	1984 Mar 15	5775.1	0.67	0.10	66	7
RU Cyg	SRa	234	M6e	m-	1984 Mar 16	5776.1	0.57	0.07	95	4
W Cyg	SRb	131	M4e	m-	1984 Apr 8	5799.1	—	0.07	113	4
R Hya	M	388	M6.5e	m-	1983 Dec 24	5693.0	0.47	0.07	177	4
W Hya	SRa	382	M8e	m	1985 Jul 2	6248.6	0.37	0.07	89	4
R Leo	M	313	M7e	m+	1982 Nov 26	5300.1	0.64	0.07	172	1
X Oph	SRa	334	M6.5	m-	1976 Jun 20	2949.7	0.53	0.08	71	1
U Ori	M	372	M6.5e	m	1984 Apr 21	5811.5	0.47	0.07	142	4
SV Peg	SRb	145	M7	m-	1984 Mar 22	5782.2	—	0.07	90	4
ST Sgr	M	395	S7/3e	s	1989 Jul 13	7690.9	0.56	0.07	70	
IK Tau	M	460	M6e	m+	1976 Jul 24	2983.7	0.47	0.08	98	4
S UMa	M	226	S2/6e	m-	1981 May 18	4742.7	0.42	0.14	88	
R Vir	M	146	M3.5e	m+	1985 Jul 3	6249.6	0.60	0.14	98	5

Table 3. Additional Time Series Spectra of χ Cygni

Date	Julian Date (2440000+)	Phase	Resolution (cm^{-1})	S/N
1984 Jun 18	5870	0.07	0.07	45
1984 Sep 5	5949	0.22	0.07	168
1985 Nov 6	6377	0.29	0.07	88
1984 Nov 1	6006	0.41	0.07	65
1984 Dec 9	6044	0.50	0.07	101
1986 Feb 17	6479	0.54	0.07	112
1985 Feb 11	6108	0.63	0.07	142
1985 Apr 2	6158	0.76	0.07	140
1985 May 1	6187	0.83	0.07	67
1985 Jun 26	6243	0.97	0.07	75
1985 Jul 2	6249	0.98	0.07	138

All the spectra were observed with one of two Fourier transform spectrometers at the coudé focus of the Kitt Peak 4 meter telescope. Observations prior to October 1978 were obtained with a prototype spectrometer similar to the instrument described by Ridgway & Capps (1974). The remainder of the spectra were observed by the facility spectrometer described by Hall et al. (1979). Adequate discussion of the instrumentation and general characteristics of the data may be found in the papers listed above. We re-emphasize that the photometric accuracy and frequency calibration of spectra obtained with the FTS are limited by noise rather than instrumental characteristics. Frequencies are referenced to the spectrometer's laser frequency and after correction for the index of refraction of air, the spectral frequencies require only the addition of a small ($\lesssim 1\,\mathrm{km\,s^{-1}}$) correction for collimation differences between the reference and signal beams.

All spectra discussed in this paper have been apodized by function I2 of Norton & Beer (1976). Apodizing damps the wings of the intrinsic sinc function FTS instrumental profile, creating an instrumental profile similar to that of a grating spectrograph. In this process the apodizing function lowers the resolution and increases the signal-to-noise ratio. The prototype

FTS suffered from instrumental apodization resulting from systemic variation in reimaging with path difference. This results in the resolution being slightly lower than the theoretical value presented in Table 2 for the 1976 and 1977 observations.

All velocities in this paper are heliocentric. Velocities listed for lines are from the line core. Accuracies per line are better than 0.5 km s^{-1}. Measurement techniques are described by HHR.

4. Analysis

4.1. Detection

The 2 μm spectra of Miras, while not as badly blended as the visual spectra of these stars, nevertheless contain a large number of lines, most of which are relatively weak, having central depths less than $\approx$ 20%. The challenge in identifying H_2 is to unambiguously select the H_2 lines against this background. For molecules previously identified in these spectra, such as CO, CN, H_2O, or SiO, identification is a tractable problem because hundreds of lines are contributed by the species being searched for. However, the number of well placed H_2 lines (Table 1) provides a meager selection. A worst case is that encountered by Tsuji (1983) where the column density of H_2 is near the detection limit with the result that only a detection of S(1) is likely.

As a first step in identification, the spectra listed in Table 2 were plotted in the regions of the H_2 1-0 S(0), S(1), and S(2) line. Two groups of strong atomic lines, neutral titanium from the a^5P-z^5D transition and neutral scandium from the a^4F-z^4D transition, lie within a few wavenumbers of the S(0) line. These atomic lines were included in the plots which extended from 4485-4500 cm^{-1}. In cool giants the S(0) region is blanketed with weak features, presumably H_2O in the oxygen rich stars and CN in the carbon rich stars.

Using the molecular lines which are present in the 4485-4500 cm^{-1} plots (but ignoring the candidate H_2 lines), the objects in Table 2 can be sorted into five categories with nearly identical spectra shared between the stars in each category. The five categories are strong H_2O, moderate H_2O, weak H_2O, weak H_2O/CN, and strong CN. The relation to the normal classifications is obvious: strong-moderate H_2O equals to M-type, weak H_2O-weak H_2O/CN equals to S-type, strong CN equals to C-type. Due to the multidimensional aspect of classification in late type stars (temperature, luminosity and abundance), the Keenan spectral classification, especially among the S-stars, does not necessarily map into C/O abundance (Smith & Lambert 1990). As a result we have found the above classification scheme to be quite useful for the following analysis. The assigned classification category is listed on Table 2. This classification demands comparison of spectra at similar phases since the strength of H_2O depends on phase. Note that there are occasional surprising differences between the category we have assigned and the published spectral type. Fig. 1 illustrates some representative spectra.

Continua have been set by examining the highest point in each 5 cm^{-1} interval over the spectral interval observed. Detailed inspection of particular spectral regions shows that this technique produces a consistent continuum level. However, for the strong or moderate H_2O spectra the assigned continua are no doubt below the true (i.e. without atomic and molecular lines) continuum level. If the Sc I and Ti I lines in the 4400-4500 cm^{-1} region are assumed to have similar central depths in both M-type and S-type Miras, then the continuum in the M-type Miras must be well above any existing continuum point in the high resolution 2 μm spectrum. Two micron region atomic lines in S-type Miras have line depths that are relatively constant from phase 0.20 to 0.80. Again if we assume that the atomic lines in the M-type Miras do not weaken near minimum light then the continuum must be placed well above any continuum point in the spectrum at these phases to keep the atomic line depths constant. This is in agreement with water calculations provided by e.g. Aringer et al. (1997).

As can be seen from Fig. 1, the H_2 1-0 S(0) line is an obvious spectral feature in the S-type minimum light Mira spectra. In the spectra with water vapor present, S(0) is also present but due to the large amount of line blanketing present, the line is not obvious. In the Mira spectra with the strongest H_2O lines, the H_2 S(0) line cannot be identified because of strong blending with the H_2O (0,1,1)[18,9,9]-(0,1,0)[17,7,10] line at 4498.027 cm^{-1} (Zobov et al. 2000[1]). Due to these difficulties, identification of H_2 in these stars is based on consistency between the 1-0 S(0) and S(1) lines. While the H_2 line appears to weaken as C/O decreases from 1, the strength of the H_2 line is difficult to quantify because of uncertainties in the continuum and blending. In carbon rich Miras, line blanketing from CN and possibly polyatomics and scattering of the photospheric spectrum in the circumstellar dust obliterates the recognizable line spectrum and no comment on the existence of the H_2 can be made.

Identification of the H_2 may be secured by measuring consistent line strengths and velocities among the various lines predicted to be present. In the S-type Miras with the strongest H_2 lines in our sample (R And, X And, T Cam, χ Cyg, R Cyg, and ST Sgr) all the H_2 lines appearing in Table 1 are clearly identifiable and have intensities consistent with the oscillator strength and a 2000-3000 K excitation temperature. The S-type Mira spectra are particularly easy to work with, not only because of the strength of the H_2 features but also because there are few blending features. The S(0) line is the freest from blending in all spectral types. However, in the S-type stars S(1) is best for monitoring because it is not blended in S-stars and is much stronger than S(0).

Velocities of the line cores and depths of the observed H_2 lines are presented in Table 4 for the spectra where hydrogen lines could be definitely identified. For the other stars we give an upper limit of the line depths. In Table 5 velocities for groups of Ti, CN, high excitation 2-0 CO, and low excitation 2-0 CO lines are listed. The velocity agreement between the Ti, CN, and high excitation CO is generally good. Note that while the lines in each atomic/molecular group have similar central depths, the three groups cover a large range in central depth (average central depth is listed in Table 5). We have not listed the central depth of the CO low excitation lines since these lines are blends of

[1] http://www.tampa.phys.ucl.ac.uk/

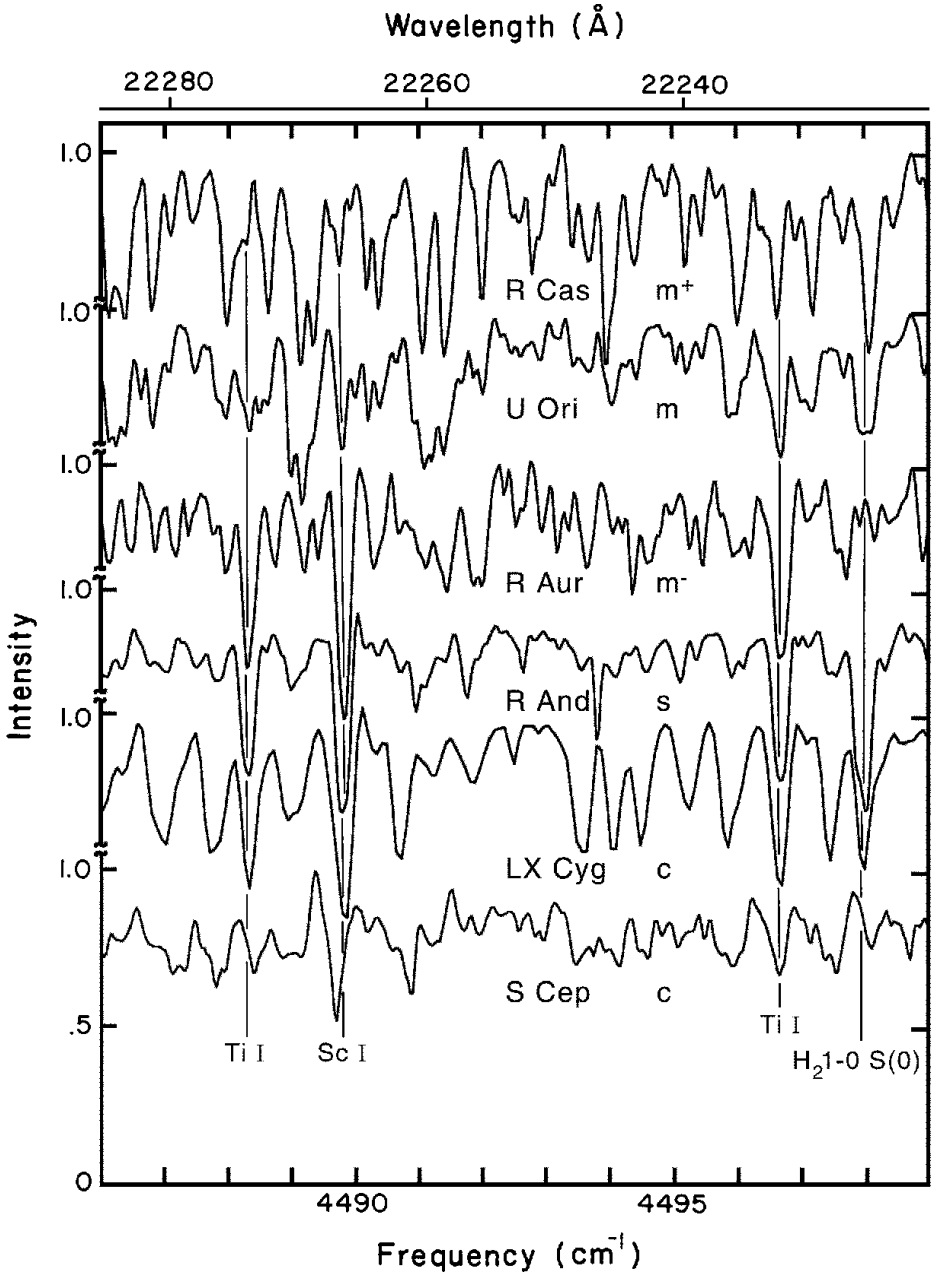

Fig. 1. Typical spectra in the 4486-4499 cm^{-1} region. The spectra range from having strong H_2O with no detectable CN (R Cas) through weak H_2O and weak CN (R And) through strong CN with no detectable H_2O (LX Cyg and S Cep). The classification according to the scheme described in the text is given for each star (see also Table 2). The strong line close to the position of the H_2 line visible in R Cas and U Ori is due to H_2O. Note the variations in strength of the atomic lines (marked) compared to the molecular lines. Spectra have been shifted to place the lines at laboratory frequencies.

multiple velocity components (HHR). The CO low excitation lines typically have central depths in excess of 70% in late M giants.

The H_2 velocities are shifted by as much as $-9\,km\,s^{-1}$ ($\lesssim 0.1\,cm^{-1}$) from the velocities of the Ti, CN and high excitation CO lines. The precision with which the laboratory frequencies are known for all these species rules out a velocity shift as the result of the laboratory data. Tsuji (1983) noted a shift of $-5\,km\,s^{-1}$ ($0.08\,cm^{-1}$) between the predicted and observed position of the H_2 S(1) line in a number of non-Mira M giants. Based only on the S(1) line he concluded that the line present was not H_2 but an unidentified line near the S(1) frequency. However in our data the strength and number of H_2 lines present make the identification secure. We conclude that Tsuji's line is indeed H_2 S(1) and that his predicted position based on hydrostatic model atmospheres does not account for velocity fields in the atmosphere. The effects of velocity fields on line profiles and positions are described in Windsteig et al. (1998) and Aringer et al. (1999). Tsuji's observations in SR type variables are consistent with our data. The cause of the velocity shift between H_2 and other lines will be discussed below.

4.2. Phase dependent behavior

4.2.1. Central depths

Fig. 2 presents the phase dependent absorption central depth of S(1) as a function of visual light phase in χ Cyg. The figure combines measurements from the spectra of HHR with those

Table 4. Observed H_2 Lines. The table lists the depth (percent measured below the continuum; D) and the heliocentric velocity (RV) of each line. For several stars we could measure only upper limits due to blending of the H_2 line with an H_2O line.

Star	1-0 S(0)		1-0 S(1)		1-0 S(2)		1-0 S(6)		1-0 S(7)		2-1 S(1)		2-1 S(2)	
	D	RV	D	RV	D	RV	D	RV	D	RV	D	RV	D	RV
R And	70	−22.7	83	−22.6	79	−22.5	54	−14.3	63	−17.1	48	−15.5	35	−13.7
X And	57	−3.6	89	−3.4	74	−4.0	...	...[a]	...	...[a]	39	−3.2	21	−3.6
R Aql	<19	...	<57	...	...	...	...	...	...	...	...	...	...	...
V450 Aql	7	−56.3	18	−57.0	...	...	...	...	...	...	...	...	...	...
R Aqr	<19	...	<53	...	...	...	...	...	...	...	...	...	...	...
R Aur	...	...	46	4.2	...	...	...	...	...	...	...	...	...	...
T Cam	52	−10.7	83	−11.2	75	−10.9	...	...[a]	...	...[a]	40	−9.4	25	−9.0
R Cas	<25	...	<59	...	...	...	...	...	...	...	...	...	...	...
SV Cas	< 6	...	31	−16.0	...	...	...	...	...	...	...	...	...	...
T Cas	>28	...	47	−12.7	...	...	...	...	...	...	...	...	...	...
W Cas	34	−42.7	74	−43.5	...	...	...	...	...	...	...	...	...	...
WZ Cas[b]	31	−30.8	66	−31.2	...	...	...	...	...	...	...	...	13	−32.1
S Cep[c]	...	...	...	...	...	...	...	...	...	...	...	...	...	...
T Cep	...	...	46	−16.7	...	...	...	...	...	...	...	...	...	...
o Cet	<32	...	<54	61.6	...	...	...	...	...	...	...	...	...	...
χ Cyg	55	−2.1	79	−3.4	75	−4.1	65	3.9	50	−1.8	41	2.5	32	−0.8
LX Cyg	48	−36.4	78	−36.6	66	−35.5	...	...[a]	...	...[a]	...	...	...	...
R Cyg	80	−21.9	95	−24.5	90	−22.3	...	...[a]	...	...[a]	53	−22.0	29	−21.2
RU Cyg	...	...	31	−11.8	...	...	...	...	...	...	...	...	...	...
W Cyg	...	...	26	−23.5	...	...	...	...	...	...	...	...	...	...
R Hya	...	...	43	−16.9	...	...	...	...	...	...	...	...	...	...
W Hya	<6	...	<45	...	...	...	...	...	...	...	...	...	...	...
R Leo	...	...	<51	3.4	...	...	...	...	...	...	...	...	...	...
X Oph	...	...	38	−77.2	...	...	...	...	...	...	...	...	...	...
U Ori	<38	...	<54	...	...	...	...	...	...	...	...	...	...	...
SV Peg	...	...	34	−8.5	...	...	...	...	...	...	...	...	...	...
ST Sgr	62	43.7	83	42.3	76	41.2	...	...[a]	...	...[a]	45	48.8	35	46.7
IK Tau	<20	...	<59	...	...	...	...	...	...	...	...	...	...	...
S UMa	25	−2.7	57	1.0	39	1.6	...	...[a]	...	...[a]	...	...	...	...
R Vir	...	...	<45	...	...	...	...	...	...	...	...	...	...	...

[a] Outside spectral bandpass of observation.
[b] For 1979 Jul 6. On 1984 Oct 14 S(0) $\leq$18%, S(1) $\leq$42%.
[c] H_2 may be present, but the line is heavily blended.

of Table 3. χ Cyg (S7,1e) will be discussed in detail because of the extensive time series of spectra available, although H_2 lines are not as strong in this star as in "pure" S-type Miras. In χ Cyg the S(1) line appears at about phase 0.0 and strengthens rapidly (the central depth increases nearly 0.5% per day) to an 80% deep line at phase 0.4. The line starts to weaken after about phase 0.6, becoming too weak to differentiate from the weak background lines between phase 1.0 and 1.3. Note, that in Fig. 2 phase 1.0 denotes the next visual light maximum. Near maximum light the line is doubled, i.e. seen at two velocities in the spectrum. Doubled spectral lines near maximum light have been observed in spectral lines of many atomic and molecular features (e.g. HHR) and is a feature found also in dynamical model atmospheres (Windsteig et al. 1998). In summary, H_2 can be seen in the spectrum throughout the light cycle with the line strongest near phase 0.5. Near maximum light H_2 lines are weak and doubled in the spectrum of χ Cyg.

Time series of three oxygen rich Miras, R Cas, T Cep and o Cet, also were examined to determine when the H_2 S(0) and S(1) lines were at maximum strength. In all cases the H_2 lines are deepest at phase 0.60. In R Cas and o Cet H_2 lines are very blended with H_2O but seem to have phase dependent behavior similar to χ Cyg.

Changes in line strength of the H_2 lines during the stellar light cycle are not limited to Mira variables. Lambert et al. (1986) noted the abnormally strong H_2 in the SRa carbon star WZ Cas. When we re-observed this star the H_2 S(0) line was not detectable, with a line depth at most half of the previous value. Both spectra are of high quality and both were obtained on the same spectrometer at the same resolution. An accurate light curve does not exist for this star, but measurements in the AAVSO archive suggest, that the first observation was obtained at a light minimum and the second one close to the light maximum.

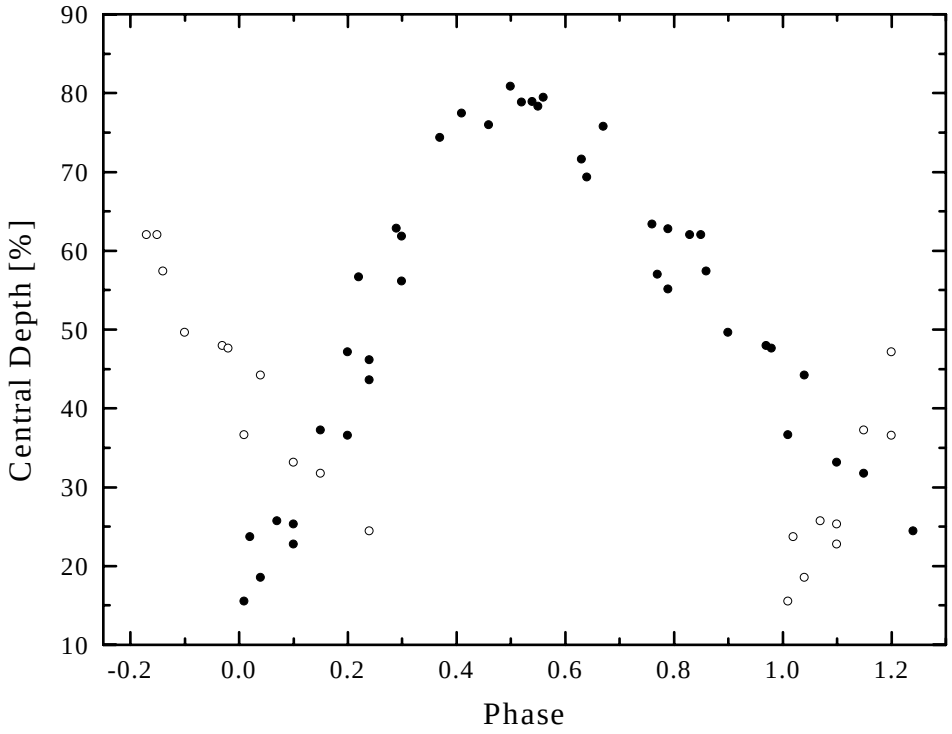

Fig. 2. Central depth as a function of visual light phase for the H_2 S(1) line in χ Cyg. The H_2 S(1) line has two well separated velocity components from approximately phase 0.1 before maximum light to 0.2 after maximum which are marked by full and open circles, respectively.

Table 5. Atomic and Molecular Line Measurements. The table lists the depth (D) and the heliocentric velocity (RV) of each line. Stars for which the H_2 line gave only an upper limit (see Table 4) are not included.

Star	Ti		CO			CN	
			low excitat.		high		
	D	RV	RV	D	RV	D	RV
R And	59	-14.5	-15.3[a]	54	-14.2	26	-13.7
X And	56	-4.3	-4.0	46	-4.4	24	-5.7
V450 Aql	60	-50.9	-50.8	39	-51.4	13	-50.9
R Aur	62	12.3	-3.2[a]	51	12.2	<22	...
T Cam	68	-8.9	-12.1	51	-8.9	20	-9.5
SV Cas	59	-11.4	-13.2	36	-10.9	16	-11.7
T Cas	54	-7.1	-11.3	47	-6.6	28	-9.4
W Cas	63	-41.0	-46.4	47	-41.1	40	-40.5
WZ Cas[b]	72	-31.6	-33.9	59	-30.7	52	-31.8
T Cep	56	-12.8	-14.9	43	-10.8	21	-13.1
χ Cyg	62	0.1	-4.7	57	-0.1	29	-1.7
LX Cyg	58	-31.1	-38.7	42	-29.4	40	-28.3
R Cyg	66	-20.9	-30.0[a]	51	-22.4	20	-30.5
RU Cyg	62	-7.4	-9.5	44	-7.5	18	-7.8
W Cyg	55	-19.1	-18.1	41	-18.4	12	-18.1
R Hya	55	-13.7	-14.4[a]	45	-13.3	<20	...
X Oph	49	-71.0	-75.4	36	−70.2	23	-70.8
SV Peg	60	-4.7	-7.2	41	−4.6	20	-6.0
ST Sgr	61	47.2	44.6	59	47.5	33	48.0
S UMa	55	1.9	3.2	40	3.1	24	4.3

[a] Double lined, weaker component RV=−22.1 R And; 12.7 R Aur; −24.0 R Cyg; −5.1 R Hya.
[b] 1979 Jul 6.

4.2.2. Velocity

Fig. 3 shows the velocity of the S(1) line in χ Cyg as a function of phase along with that of the neighboring (in frequency) Ti I lines. The behavior of the lines of both species is typical for infrared lines in Miras (HSH; Hinkle & Barnes 1979b). The H_2 velocity curve, to a first approximation, duplicates the Ti I velocity curve shifted by 0.1 in phase. Fig. 3 also indicates a slight difference in slope between the Ti or CO velocity curve and the H_2 velocity curve.

Both depth and velocity information as well as line profile information may be displayed three dimensionally, as contours of intensity with velocity (or frequency) as one axis, and phase as the other axis. Figs. 4 and 5 display H_2 S(1) and Ti I 4488.3 intensity-velocity-phase contour maps for χ Cyg. Features noted in Fig. 1 may be seen in the contour plots. Note in particular that the H_2 originates later than the Ti in a light cycle. When the H_2 appears it has nearly the same velocity as the Ti but as phase increases the velocity becomes more negative compared to the Ti. In the description of the velocity as a function of phase (Fig. 3) this effect was represented by a phase shift of about 0.1 with a change of slope between the H_2 and Ti velocity curves.

4.2.3. Line profiles

Figs. 4 and 5 provide another dimension of information since the intensity information, i.e. the line profiles, is plotted. The H_2 S(1) line is broader than the Ti I line. The lines of both Ti and H_2, but particularly H_2, are asymmetric. In χ Cyg, the positive wing is noticeably broader than the negative wing. Both the H_2 and

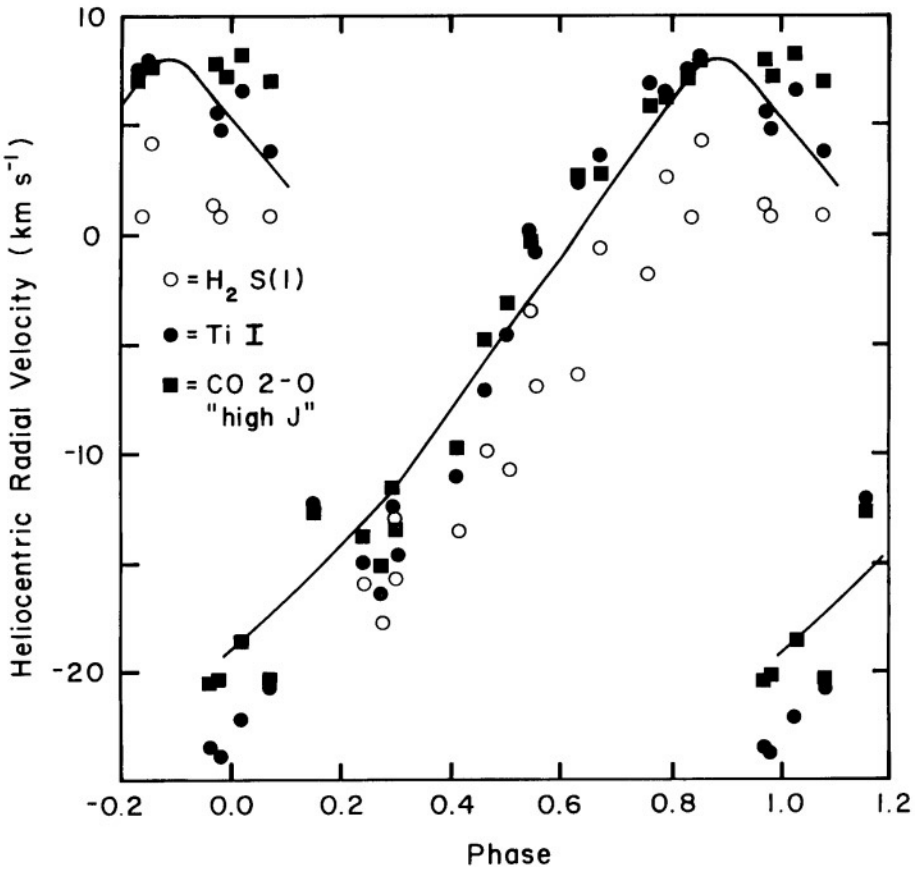

Fig. 3. Radial velocity as a function of phase from the deepest point in the line profile for the H_2 1-0 S(1), CO 2-0 high J", and Ti I lines in the 2 μm spectrum of χ Cyg. The solid curve is representative of the CO Δv=3 velocity curve (HHS) from the 1.6 μm spectrum. Note the significant departure of the H_2 velocities from the relation established by the other three groups of lines.

the Ti lines have inverse P-Cygni line profiles between phases $\approx$ 0.7 and 1.10. In the case of χ Cyg the emission is not strong.

To further investigate the cause of the line asymmetry we have examined the HSH R And time series spectra. R And has very strong H_2 lines. In Figs. 6 and 7 a time series of S(1) line profiles for the S-type Miras χ Cyg and R And are presented. In R And the asymmetry, seen in the χ Cyg lines at phases 0.3 through 0.8, is even more marked. The R And S(1) line cores show a strong asymmetry. An additional asymmetry is caused by the near maximum light emission negative of the S(1) and Ti absorption lines, which is present in χ Cyg at a phase as early as 0.8. In R And the emission in the Ti line is observed at phase 0.8, too, while the emission in the H_2 line is not detectable before light maximum.

In Figs. 6 and 7 we include a line profile of a low excitation CO line ($^{12}C^{16}O$ 2-0 R21) as well as a high excitation H_2 line (1-0 S(7)) and a Ti line. In both stars the S(1) line profiles are similar in breadth and velocity to the low excitation 2-0 CO line profiles. In the preceding section we noted in our sample of $>$20 stars the agreement of velocities between H_2 S(1) and the low excitation 2-0 CO lines. The H_2 S(7) line is similar to the Ti line.

4.3. Line intensities

In order to investigate the dependence of H_2 intensity on the intensity of metal lines and C, N, O group lines, a representative set of lines from Ti, CN, and CO were measured (Table 5). As a first approximation, the average depth of each group of lines was used as an index. In stars with strong H_2O and strong CN, blending reduced the line list to less then a usable number of lines. The strong H_2O and strong CN stars will not be discussed below. Among the remaining stars, which cover a restricted range in C/O, the Ti, CO, and CN line strengths are fairly well correlated. H_2 is not correlated with these line strengths.

In Fig. 8 the H_2 S(0) central depths are plotted as a function of period. At a given period, S and SC stars show stronger H_2 lines than M stars. Therefore we note that a higher C/O ratio leads to stronger H_2 lines. The period of the Mira, shown by Keenan (1966) to be related to the temperature, is a second factor. Over the range of periods examined, P$\approx$200 to 500 days, we find that long period is a necessary condition for strong H_2 lines.

The envelope of points in Fig. 8 suggests that for C/O=1, the H_2 S(0) central depth increases by $\approx$20% for each 100 day increase in period. The line saturates at a period of about 400 days. The data suggest that the H_2 line strength among the Miras can be parameterized as a set of lines parallel to this relation, with each line being defined by the C/O. However, more data on C/O and more measurements of H_2 lines are needed to confirm this.

Of course, one has to be aware that H_2O can severely modify the height of the continuum and may therefore influence this relation between intensity and C/O.

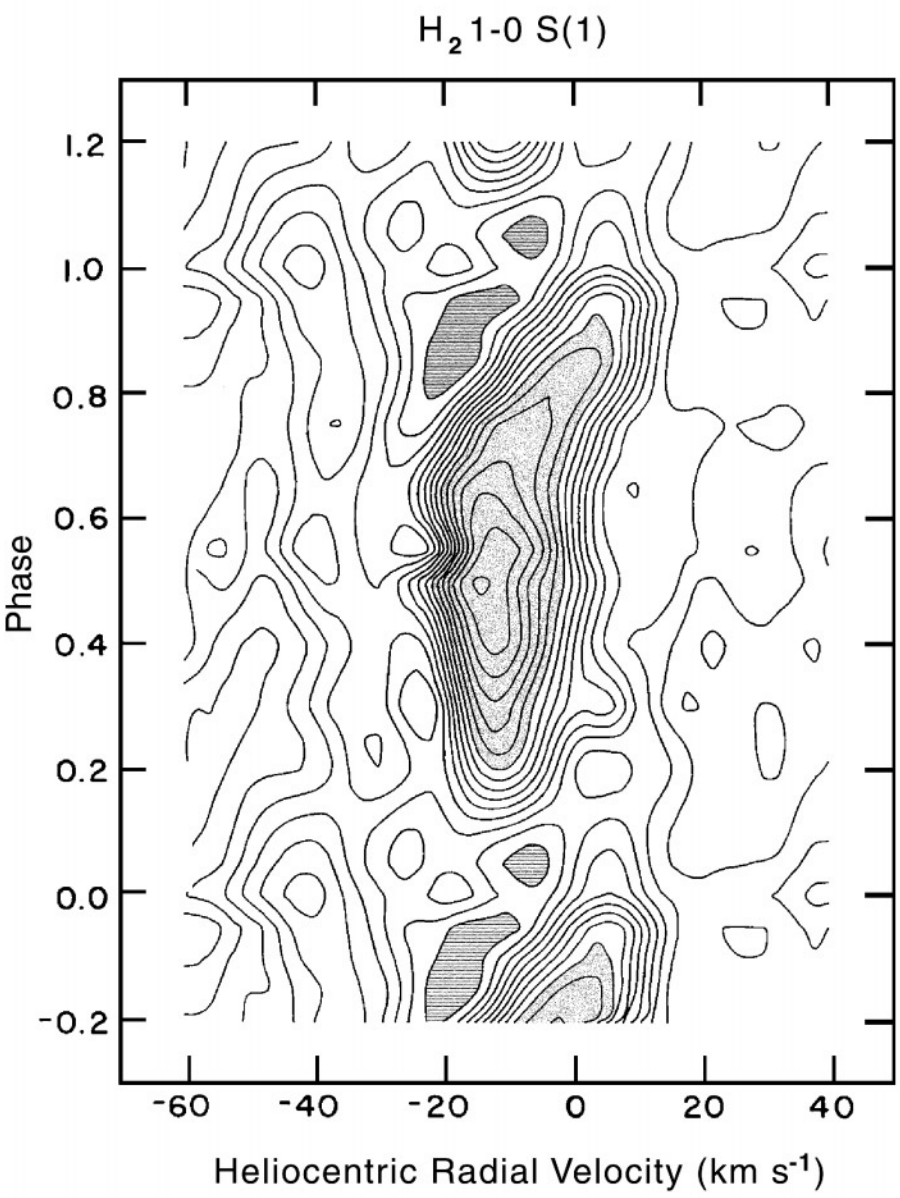

Fig. 4. Intensity contours as a function of phase and velocity for H_2 1-0 S(1) in the χ Cyg spectrum. Contours are in steps of 5% in intensity. For orientation the areas representing 50% or less intensity are dotted, while the areas with 90% or more intensity are shaded. Note that the S(1) line is only weakly present in absorption at phase 1.0-1.1 with weak emission at $\approx -10\,\mathrm{km\,s^{-1}}$ from the absorption.

5. Discussion

5.1. Dynamic atmosphere scenario

To understand the behavior of the H_2 in Miras it is necessary to start by briefly reviewing the scenario presented in previous papers to explain the features observed in the infrared spectrum (HHR; Fox et al. 1984). Velocity curves of the type measured for H_2 and other infrared lines are indicative of an overall stellar pulsation with a shock leading the passage of each pulse through the stellar atmosphere. The pulsation cycle equals the length of the light curve, a period on the order 1 year for a typical Mira. The shock emerges in the infrared photosphere in the premaximum phases. As the shock propagates through the atmosphere the spectrum shows a progressive weakening of lines in the cool, inwardly moving gas. At some phase near maximum light the gas below the shock develops a sufficient column density to be detectable. These lines sample the hot, outwardly moving gas of the next pulse. Hence the observation of doubled spectral lines, with velocities both toward and away from the stellar center-of-mass velocity, exists only after the shock has propagated through a considerable fraction of the stellar atmosphere.

In addition to the above region, which contributes most of the infrared spectrum, Mira atmospheres have a complex, extended structure. This region of the atmosphere can be probed in a variety of strong, low excitation atomic and molecular lines (e.g. HHR). The infalling photospheric layers, seen in the infrared at maximum light, persist well into the next light cycle. At least two distinct circumstellar regions are also present. A pseudo-static, $\sim$1000 K molecular region (Ridgway & Friel 1981; Tsuji 1988)[2] and an expanding, $T_{exc} \approx 100$ K, classical circumstellar envelope.

[2] To avoid confusion we note that this is the layer denoted as "800 K component" in HHR.

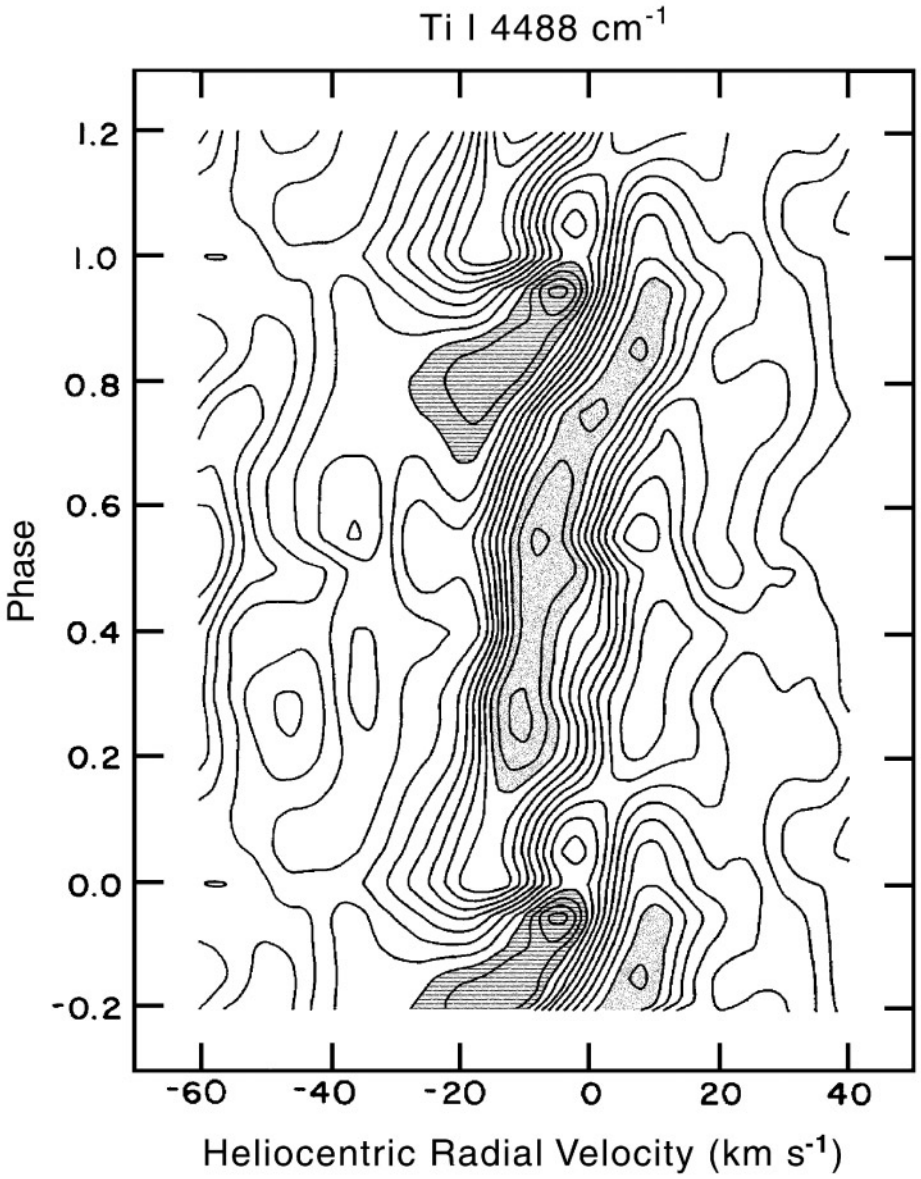

Fig. 5. Intensity contours for the Ti I line at 4488 cm^{-1} in the χ Cyg spectrum. Note, compared to Fig. 4, the conspicuous presence of a two absorption velocity components at phases 0.9-1.1, the strong emission between the components, and the narrowness of the Ti line relative to the H_2 line.

5.2. H_2 lines

We will focus in the discussion on the M and S type stars. Carbon stars are discussed in Johnson et al. (1983). The above description of the behavior of photospheric lines characterizes the general behavior seen in the H_2 lines. The interesting feature of the H_2 lines is how their behavior differs from that of other spectral lines. Comparison will be made to CO lines, which are arguably the best infrared spectroscopic probe of the atmosphere. The Δv=3 transition has weak spectral lines so that only atmospheric regions near the continuum forming layers are probed. The high excitation lines of the stronger Δv=2 transition probe similar atmospheric regions. The low excitation CO Δv=2 lines cover extended regions of the atmosphere.

Four aspects of the behavior of the H_2 lines need to be explored:

– In the spectra of Miras, especially those with stronger H_2, the H_2 lines are notably asymmetric.
– For Mira variables the H_2 lines initially appear (at $\phi \approx 0.0$) at a velocity near that of CO Δv=3 or Ti. They later appear shifted to negative velocities compared to the CO Δv=3 and Ti lines. For small amplitude variable stars the H_2 line core is velocity shifted relative to atomic lines in that spectral region.
– For Mira variables H_2 lines undergo much more extreme phase dependent intensity changes than lines of other molecules like CO or OH.
– For Mira variables the H_2 lines develop negatively shifted emission near maximum light.

A fraction of the asymmetry and velocity shift can be explained by the low molecular weight and small absorption coefficient of the H_2 molecule. H_2 weighs 1/14 of CO and 1/24 of Ti, small enough that thermal velocities can be several times larger than the typical cool star microturbulence of a few kilometers per second (Lambert et al. 1986). However, the stronger

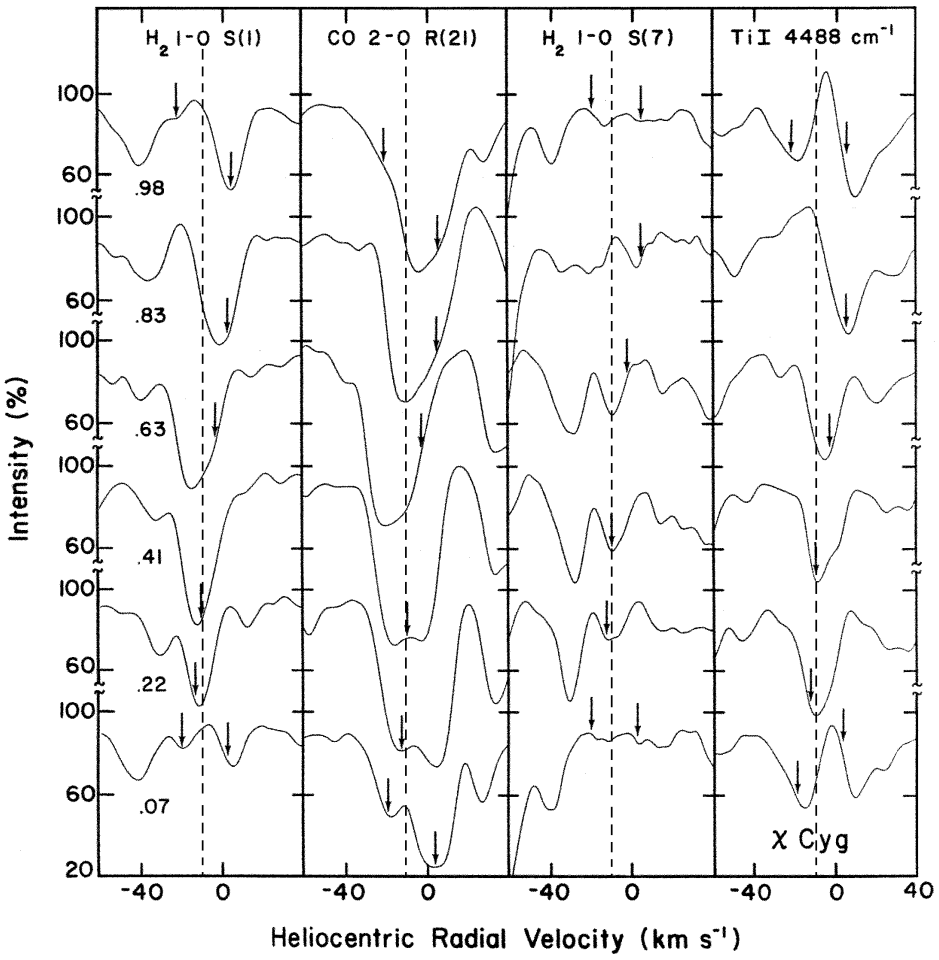

Fig. 6. Time series of line profiles in χ Cyg as a function of phase for (left to right) H_2 1-0 S(1), CO 2-0 R(21), H_2 1-0 S(7), and Ti I 4488 cm^{-1}. The dotted line marks the center-of-mass velocity. The arrows above the spectrum locate the CO Δv=3 photospheric velocity. Phase is labeled under the S(1) spectrum. Note the emission at phase 0.83 and 0.98 in the S(1) and Ti lines. Time increases upward.

lines in Miras have FWHM of $\approx$20 km s^{-1}, far in excess of the microturbulence, so the thermal broadening has a small rather than large impact on the total line width in these stars.

5.2.1. Line profile

The similar shapes of the low excitation CO and H_2 profiles seem to imply that low excitation H_2 lines, like low excitation CO lines, are formed over an extended atmospheric region (e.g. HHR). In the case of CO there is considerable evidence from velocities and excitation temperature that strong, low excitation CO lines are formed throughout the atmosphere. The evidence for H_2 is more circumstantial. The H_2 line profiles are those expected from a very strong line formed in a dynamic atmosphere. Importantly, however, the line nearly disappears at maximum light, suggesting that most of the contribution to the lines occurs in the dynamic part of the atmosphere rather than the stationary molecular layer.

As expected for a line formed high in the atmosphere, the velocity of the S(1) line relative to photospheric lines differs from star to star. In Tables 4 and 5, the S(1) line velocity is for some stars equal to the photospheric velocity as measured from CN, Ti, or high excitation Δv=2 CO. For other stars the S(1) velocity matches that of the COΔv=2 low excitation lines. In other cases it is in between these or even more displaced from the photospheric velocity than are the low excitation CO lines.

5.2.2. Resonant scattering and postshock recombination

Schmid-Burgk & Scholz (1975) and Schmid-Burgk et al. (1981) demonstrated that M giant and supergiant atmospheres are extended. In the case of pulsating late-type stars, Jones et al. (1981), Ukita (1982), Bowen (1988), and Bessell et al. (1989) have shown that the atmosphere becomes extended by an additional factor of at least 2. HHR, Hinkle & Barnes (1979a,b) and Bessell et al. (1989) have shown that a large atmospheric extent compared to the stellar radius appears necessary to explain the behavior of the infrared CO lines, infrared atomic lines, and H_2O bands in Miras.

In an extended atmosphere, a non-negligible contribution could be made to the line profile from gas beyond the photospheric limb. The spectrum from this gas contributes emission to the line profile as continuum photons undergo resonant scattering and are redirected into the line of sight. The gas over the limb has a very small velocity component from stellar pulsation along the line of sight and emission appears near the center-of-mass velocity. The observed emission, strongest near maximum light, is asymmetric presumably because it covers and partly fills the

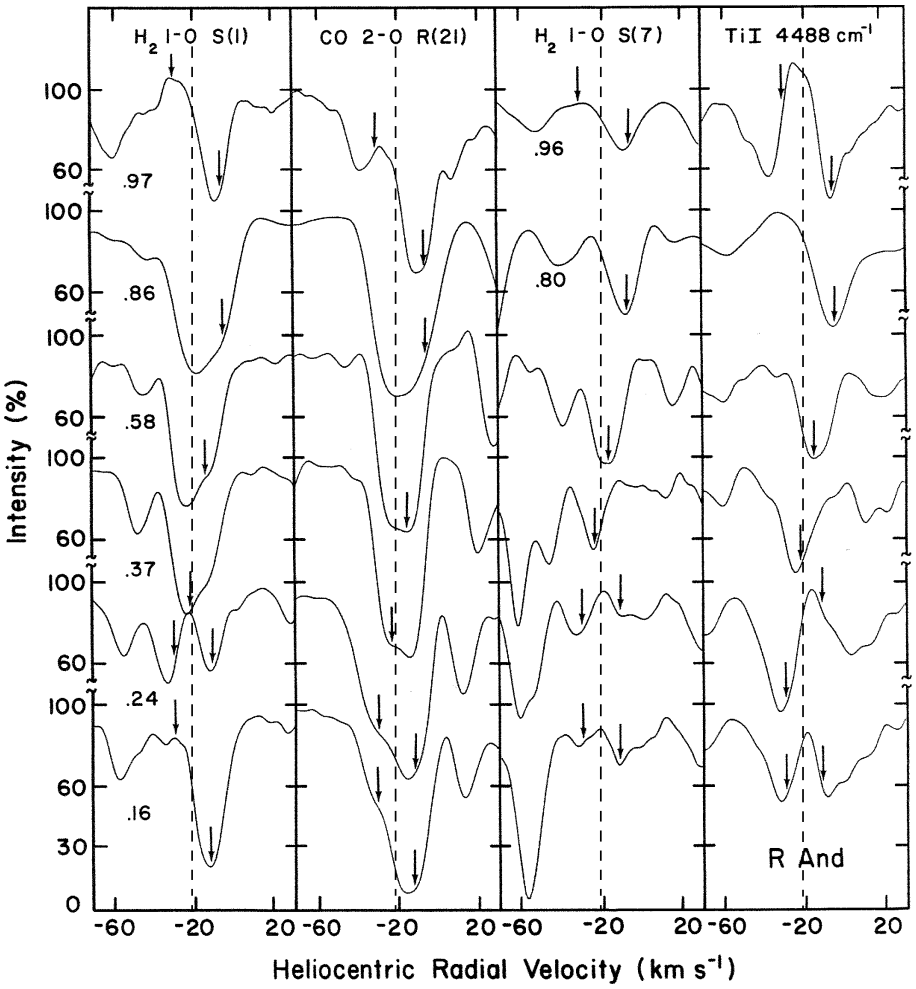

Fig. 7. R And line profiles. Spectra taken at phase 0.86 and 0.97 did not include the S(7) line. This line is shown at the slightly different phases 0.80 and 0.96.

absorption line. The emission appears near, or slightly negative of the center-of-mass velocity ($-19\,\mathrm{km\,s^{-1}}$ for R And [Lo & Bechis 1977]; $-8\,\mathrm{km\,s^{-1}}$ for χ Cyg [Lo & Bechis 1977; Knapp et al. 1982]).

Fox et al. (1984) and Gillet (1988) have shown that the atomic hydrogen line emission, conspicuous in the near maximum light spectra, is the result of recombination behind the shock. Hinkle & Barnes (1979b) suggested that infrared atomic emission lines also could be explained by recombination behind the shock. However, in the case of H_2, the very small oscillator strength and low density of the Mira atmosphere requires recombination over a path length that is too long for this scenario possibly to be correct. Furthermore rapid recombination of the H_2 would not be expected in the hot, post shock gas, where excitation temperatures in excess of 3500 K have been measured for CO (HSH). The relative contributions to the atomic emission lines from post-shock recombination and resonant scattering in the extended cool infalling gas need to be reexamined.

The resonant scattering that we propose to explain the H_2 emission is slightly different in physical origin. We propose that the H_2 profiles are formed in a spherically extended "photosphere" where resonant scattering makes a contribution to the photospheric line profile. This contribution will have velocity near the center-of-mass velocity since the resonant scattering takes place in gas seen near the stellar limb.

The contribution to the H_2 line by the classic expanding circumstellar shell generally should be negligible as a result of the low H_2 oscillator strength and the relatively modest column density expected. For example, in the case of $\dot{M} = 10^{-4}$ $M_\odot\,\mathrm{yr}^{-1}$, a mass loss rate which probably exceeds that of any star discussed in this paper by at least an order of magnitude, Keady & Ridgway (1991) predict an S(1) line 10% deep for an IRC+10216 model circumstellar shell. The circumstellar H_2 line depth will scale approximately as the mass loss rate since the lines are unsaturated.

5.3. Role in atmospheric structure

An estimate of the column density of H_2 would be revealing of the role of H_2 in the Mira atmospheres. However, there are obvious difficulties in converting the observed line profiles or equivalent widths into a column density. In the 2 μm region, lines with central depths of more than about 40% are saturated (Hinkle et al. 1976) while lines can be no stronger than about 10% to be on the linear portion of the curve of growth (Tsuji 1983). Table 4 reveals that in most cases the H_2 lines are strongly

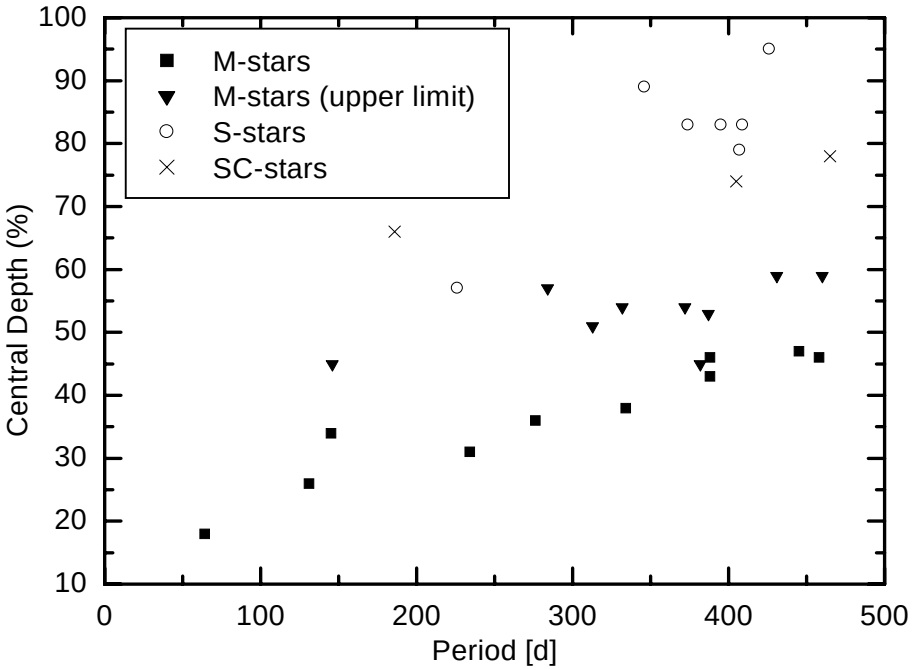

Fig. 8. The central depth of H_2 S(1) as a function of period. The filled symbols are oxygen rich stars, the open circles are S stars and the crosses mark SC stars.

saturated. Also as described above, the atmospheres of stars with H_2 are dynamic and highly extended, requiring spherical models. The complex line profile and atmospheric geometry demand detailed modeling and this will be carried out in paper II. Here we simply note that typical CO column densities of $\sim 10^{24}$ CO/cm^{-1} have been reported by HSH, so assuming solar C/H H_2 column densities of $\sim 10^{27}$ would not be unexpected.

H_2 Rayleigh scattering opacity increases as λ^4. Using the H_2 Rayleigh scattering cross section of Dalgarno & Williams (1962), optical depth greater than unity can be expected from the substantial H_2 column density present. However, in the infrared this opacity will be negligible. It follows that due to the continuum optical depth the infrared line forming region is not easily observable in the visual. The low dissociation potential H_2 molecule must be concentrated in the cooler regions of the atmosphere, so the H_2 opacity conceals even more of the atmosphere than might otherwise be assumed. We note that a large H_2 Rayleigh scattering contribution to the blue continuum is not limited to phases when the H_2 column density is at a maximum. A column density of $2{\cdot}10^{26}$ in the infrared corresponds to optical depth unity at 4000 Å. From Fig. 2, we can see that the H_2 Rayleigh scattering opacity from infalling gas near maximum light could be significant in the blue and ultraviolet even when H_2 lines are difficult to detect in the infrared. This is in agreement with the observation that the infalling outer layers of Miras are observed for a much longer time in the blue-ultraviolet than in the infrared (Hinkle & Barnes 1979b; Barbier et al. 1988).

5.4. Comparison with atmospheric models

The behavior of the H_2 absorption observed in Figs. 2 and 3 clearly shows strong variations in intensity. These are probably due to the dissociation and recombination of molecular hydrogen during the Mira variation cycle. Other effects that could modify the line intensity can be excluded for the following reasons: We found no indication of unusual effects on the line profiles, especially the line cores, that might indicate significant filling of the absorption by emission. An excitation effect would modify the profile between the different H_2 lines, but we observe the same phase dependent variation in all lines of H_2. Finally, a variation of the continuum can be excluded as well by other spectral lines, e.g. Ti lines. This significantly constrains the physical conditions in the atmosphere, and the applicability of numerical models.

From Fig. 3, it is clear that the strong and variable photospheric H_2 component arises in the post-shock gas. The delayed onset of H_2 relative to Ti and CO is most likely due to the small H_2 oscillator strength – the post shock gas column must increase to a much greater column density for detectable H_2 absorption than for Ti and CO. However, there is no evidence for a significant temporal delay in formation of H_2 relative to, for instance, CO. If the H_2 formation were significantly delayed, the absorption core might be expected to appear red shifted relative to CO and Ti, since the photospheric gas decelerates throughout the cycle. The observed appearance of the H_2 component with a relative blue shift is puzzling, until the extended geometry is considered. The observed line profile will include the sum of contributions from the absorption profile (observed against a limb-darkened source) and a most likely limb brightened distribution of emission. The emission will tend to shift the resultant absorption profile center to the blue. The apparent "phase shift" between H_2 and Ti/CO may then be due to differences in detail in the distribution and proportion of absorption and emission components. Certainly an interpretation will require careful models of the line formation, or eventually spatial resolution of the Mira surface.

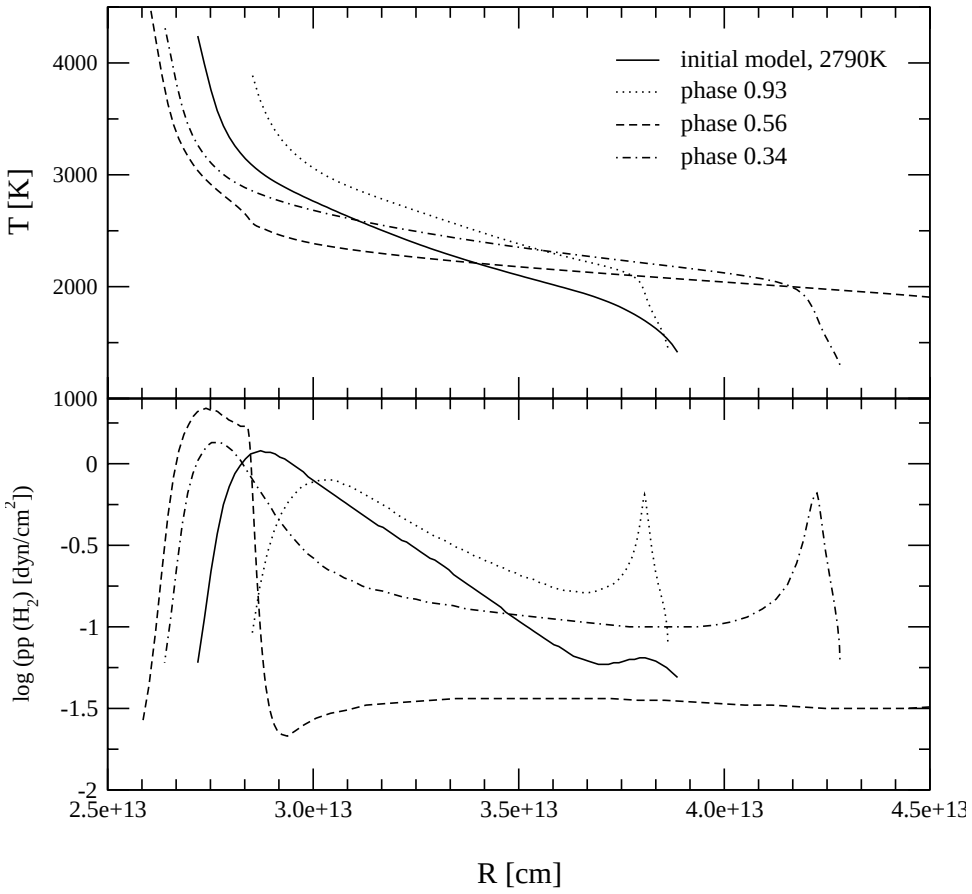

Fig. 9. Gas temperature and partial pressure of H_2 as a function of the radius for three phases (phases 0.34, 0.56 and 0.93 of the bolometric light curve) of a dynamical atmosphere calculated with a piston velocity of 2 km/s and a period of 525 d and for the hydrostatic initial model ($T_{\rm eff} = 2790\,K$, $L = 10^6\,L_\odot$).

Can the rapid formation of H_2 in the post-shock gas be understood? It has been suggested (Bowen 1988), based on the highly density dependent three-body association rates for the reaction H + H + H $\rightarrow$ H_2 + H and densities predicted by pulsation models, that molecular H_2 will not form in Mira atmospheres. This conclusion was based on models which predicted typical photospheric densities in the range 10^5 to 10^{10} H_2 cm^{-3}. The H_2 formation rate at T=2500 K would then be in the range 10^{-17} to 10^{-12} sec^{-1} cm^{-3}, and in the most favorable case the H_2 formation time would be thousands of years. However, we can now approach the question empirically. The formation of H_2 is observed to occur rapidly, in no more than 0.1 of the period, or about 40 days. At 2500 K, via three-body reaction, the required density of H is greater than or equal to 10^{12} cm^{-3}. Is this reasonable? A typical H density of 10^{12} cm^{-3} and a scale height of 150 $R_\odot$ would give an H_2 column of about $5{\cdot}10^{24}$ cm^{-2}. This is near the smallest H_2 column which we might expect to detect by absorption in the quadrupole lines. Hence any star in which we detect H_2 will probably have a column density consistent with a high photospheric density, sufficient for rapid H_2 formation. A corollary conclusion is that the Bowen models do not predict a photospheric density sufficiently high to describe the Mira stars observed in our program.

Latter & Black (1991) outline paths to form H_2 in addition to three body reactions. Of particular relevance to low density regions of Mira atmospheres are processes requiring either H^+ or H^-. Since the shock both dissociates H_2 and ionizes hydrogen (Fox & Wood 1985), ample H^+ will be present. Alternately, in the 3000-4000 K post shock gas the supply of free electrons guarantees H^- is present. In any case, the rapid reformation of H_2 in the cooling post shock gas does not appear to be a theoretical embarrassment.

5.5. Outlook

Dynamical model atmospheres as they have been published by Höfner & Dorfi (1997) and Höfner et al. (1998) predict quite strong temporal variations of the H_2 density. This is demonstrated in Fig. 9 where we plot the gas temperature and the partial pressure of H_2 as a function of the radius. Three phases of an oxygen-rich non-grey dynamical atmosphere (Höfner 1999) calculated with a piston velocity of 2 km/s and a period of 525 d and the corresponding hydrostatic initial model ($T_{\rm eff} = 2790\,K$, $L = 10^6\,L_\odot$) are shown. No dust has been included for the oxygen-rich stars. Due to the different atmospheric extensions and the shocks moving through the atmosphere the H_2 partial pressure changes significantly in a given radial layer. At certain phases it may be much higher or smaller than in the hydrostatic case. This will also give rise to variations of the H_2 features as they have been observed in the Mira stars. Synthetic H_2 spectra calculated from dynamical model atmospheres will be discussed in a following publication.

6. Conclusions

The vibration-rotation fundamental transition of H_2 contributes spectral lines in cool giants. In the coolest giants blending with lines of other molecules makes detection of the sparse H_2 spectrum difficult. The exception is the "S-type" giant spectra where there are few blending features and detection is easier. In all cool Miras there is evidence that strong H_2 lines are present in the spectrum; for the cool S-type Miras these lines are obvious spectral features in some cases reaching central depths of 80% with FWHM of 30 km s^{-1}. The strength, width, and velocity of the line is attributable to line formation over a great range of the stellar atmosphere. The large column density of H_2 required by these strong lines implies a large H_2 Rayleigh opacity in the blue.

In Mira variables, where the strongest H_2 lines are observed, the column density can be large. Assuming a stellar radius of 300 $R_\odot$ and a similar thickness for the stellar atmosphere, an appreciable fraction of the stellar mass is suspended in the stellar atmosphere. The H_2 lines are at most half the strength in SRa variables as in Mira variables. Assuming that stellar masses and surface temperatures are the same for similar spectral type SR and Mira variables, the H_2 line strength reflects the density and extent of the stellar atmosphere. A possible implication is that SR variables represent a higher pulsation mode than the Miras where less energy is transferred to supporting a highly extended stellar atmosphere. The transfer of energy to the stellar atmosphere occurs through the stellar pulsation. HHR found that the outward momentum flux associated with a Mira pulsation exceeds L/c by about a factor of 1000. The estimated mass and extent of the S-type Mira atmospheres requires an energy input approaching that of the stellar luminosity to support it against gravitational collapse.

Hydrogen (atomic and molecular) is the spectral diagnostic of choice in evaluating stellar atmospheres and eventually in determining the abundances. Our identification of the velocity shifted line noted by Tsuji (1983) as H_2 puts current oxygen rich giant model atmospheres in reasonable agreement with observation for the non-variable M giants. Lambert et al. (1986) reached a similar conclusion for the carbon stars. However, our results also show that even in the non-variable M and C stars extended atmospheres are required to explain the velocity of the observed H_2 line core.

Since Miras are at the final stage in evolution before ejection of the outer envelope, the abundances are of considerable significance. The complexity of computing realistic model atmospheres for the Miras is well known (Bertschinger & Chevalier 1985; Bessell et al. 1989). The H_2 line profiles demonstrate that extended, spherical model atmospheres and resonant scattering are essential in a detailed understanding the observed spectrum.

Acknowledgements. The work of BA and TL was supported by the Austrian Science Fund Project S7308. We thank M. Bessell, S. Höfner, and P. Wood for useful comments and H. Johnson for encouragement with this project. P. Bernath provided useful information on the H_2 oscillator strengths. We thank D.N.B. Hall for assistance with the early stages of this project. W. Lenz and J.C. Golson provided assistance at the telescope. V. Smith and D. Lambert graciously provided their list of CN 0-2 red system lines. This research made use of the SIMBAD database operated by CDS in Strasbourg, France.

References

Aringer B., Kerschbaum F., Jørgensen U.G., et al., 1997, In: Heras A.M., Leech K., Trams N.R., Perry M. (eds.) Proc. First ISO Workshop on Analytical Spectroscopy, ESA-SP 419, p. 249
Aringer B., Hinkle K., Lebzelter T., Windsteig W., 1999, In: Hron J., Höfner S. (eds.), Abst. of the 2nd Austrian ISO workshop, Atmospheres of M, S and C Giants. Vienna, Austria, 1999, p. 43
Barbier M., Mayor M., Mennessier M.O., Petit H., 1988, A&AS 72, 463
Bertschinger E., Chevalier R.A., 1985, ApJ 299, 167
Bessell M.S., Brett J.M., Scholz M., Wood P.R., 1989, A&A 213, 209
Black J.H., van Dishoeck E.F., 1987, ApJ 322, 412
Bowen G.H., 1988, ApJ 329, 299
Bragg S.L., Brault J.W., Smith W.H., 1982, ApJ 263, 999
Dalgarno A., Williams D.A., 1962, ApJ 136, 690
Forsberg P., 1987, The Spectrum and Term System of Neutral Titanium. Lundabygdens Acupress, Lund
Fox M.W., Wood P.R., 1985, ApJ 297, 455
Fox M.W., Wood P.R., Dopita M.A., 1984, ApJ 286, 337
Gillet D., 1988, A&A 192, 206
Goorvitch D., Goebel J.H., Augason G.C., 1980, ApJ 240, 588
Hall D.N.B., Ridgway S.T., 1977, In: Les Spectres des Molecules Simples au Laboratoire et en Astrophysique. Mem. Soc. Roy. Sci. Liege, (21st Colloque Internationale d'Astrophysique de Liege), p. 243
Hall D.N.B., Ridgway S.T., Bell E.A., Yarborough J.M., 1979, Proc. SPIE 172, 121
Herzberg G., 1938, ApJ 87, 428
Hinkle K.H., Barnes T.G., 1979a, ApJ 227, 923
Hinkle K.H., Barnes T.G., 1979b, ApJ 234, 548
Hinkle K.H., Lambert D.L., Snell R.L., 1976, ApJ 210, 684
Hinkle K.H., Hall D.N.B., Ridgway S.T., 1982, ApJ 252, 697 [HHR]
Hinkle K.H., Scharlach W.W.G., Hall D.N.B., 1984, ApJS 56, 1 [HSH]
Hinkle K.H., Wilson T.D., Scharlach W.W.G., Fekel F.C., 1989, AJ 98, 1820
Hinkle K.H., Lebzelter T., Scharlach W.W.G., 1997, AJ 114, 2686
Höfner S., Dorfi E.A., 1997, A&A 319, 648
Höfner S., Jørgensen U.G., Loidl R., Aringer B., 1998, A&A 340, 497
Höfner S., 1999, A&A 346, L9
Jennings D.E., Bragg S.L., Brault J.W., 1984, ApJ 282, L85
Johnson H.R., Goebel J.H., Goorvitch D., Ridgway S.T., 1983, ApJ 270, L63
Jones T.W., Ney E.P., Stein W.A., 1981, ApJ 250, 324
Kaler J.B., 1985, ARA&A 23, 89
Keady J.J., Ridgway S.T., 1991, ApJ 406, 199
Keenan P.C., 1966, ApJS 13, 333
Knapp G.R., Phillips T.G., Leighton R.B., et al., 1982, ApJ 252, 616
Kholopov P.N., Samus N.N., Frolov M.S., et al., 1985-88, General Catalogue of Variable Stars. 4th ed., Nauka Publishing House, Moscow [GCVS4]
Lambert D.L., Brooke A.L., Barnes T.G., 1973, ApJ 186, 573
Lambert D.L., Gustafsson B., Eriksson K., Hinkle K.H., 1986, ApJS 62, 373
Latter W.B., Black J.H., 1991, ApJ 372, 161
Lebzelter T., Hinkle K.H., Hron J., 1999, A&A 341, 224
Lebzelter T., Kiss L.L., Hinkle K.H., 2000, A&A in press

Lo K.Y., Bechis K.P., 1977, ApJ 218, L27
Norton R.H., Beer R., 1976, J. Opt. Soc. Am. 66, 259
Ridgway S.T., Capps R.W., 1974, Rev. Sci. Instr. 45, 676
Ridgway S.T., Friel E.D., 1981, In: Chiosi C., Stalio R. (eds.) Effects of Mass Loss on Stellar Evolution. D.Reidel, Dordrecht, p. 119
Schmid-Burgk J., Scholz M., 1975, A&A 41, 41
Schmid-Burgk J., Scholz M., Wehrse R., 1981, MNRAS 194, 383
Smith V.S., Lambert D.L., 1989, private communication
Smith V.S., Lambert D.L., 1990, ApJS 72, 387
Tsuji T., 1964, Annals Tokyo Astr. Obs. 9, 1
Tsuji T., 1983, A&A 122, 314
Tsuji T., 1988, A&A 197, 185
Turner J., Kirby-Docken K., Dalgarno A., 1977, ApJS 35, 281
Ukita N., 1982, A&A 112, 167
Wallerstein G., Hinkle K.H., Dominy J.F., et al., 1985, MNRAS 215, 67
Windsteig W., Höfner S., Aringer B., Dorfi E., 1998, In: Kaper L., Fullerton A.W. (eds.) Proc. ESO Workshop Cyclical Variability in Stellar Winds. Garching bei München, Germany, 1997, p. 308
Zobov N.F., Polyansky O.L., Tennyson J., et al., 2000, ApJ 530, 994